Heterogeneous–Homogeneous Interactions in Catalytic Microchannel Reactors

S. Chattopadhyay and G. Veser
Dept. of Chemical Engineering, University of Pittsburgh, Pittsburgh, PA 15261

DOI 10.1002/aic.10825
Published online March 27, 2006 in Wiley InterScience (www.interscience.wiley.com).

Micromachining of chemical reactors enables the manufacture of microchannel reactors with unsually large surface-to-volume ratios. This can strongly affect the coupling between heterogeneous (wall) reactions and homogeneous (gas-phase) reactions, ultimately leading to a complete quenching of homogeneous reactions. Using a 2D boundary-layer model coupled with detailed reaction kinetics for surface and gas-phase reactions, we investigate the ignition behavior of hydrogen/air mixtures in a Pt-coated microchannel. The influence of temperature, pressure, reactor diameter, and fuel-to-air ratio is studied. We find that a purely kinetic radical scavenging by the catalytic surface can indeed result in a complete suppression of gas-phase reactions. However, the attainability of "intrinsic safety" in microchannel reactors is strongly dependent on a fine interplay between homogeneous and heterogeneous reaction pathways in the individual reaction system. In particular, the strong dependency of homogeneous reactions on pressure leads to a breakdown of intrinsic reactor safety at sufficiently high reactor pressure. A generalized equation for the boundary of safe reactor operation is derived for the current reaction system. © 2006 American Institute of Chemical Engineers *AIChE J,* 52: 2217–2229, 2006
Keywords: catalytic hydrogen oxidation, microreactors, reactor safety, homogeneous–heterogeneous interactions, high-temperature catalysis

Introduction

The importance of heterogeneous (that is, catalytic) and homogeneous (that is, gas-phase) reactions and their interactions in particular for high-temperature catalytic reactions has been known for several decades. Margolis and coworkers were among the first to establish their role in catalytic oxidation of hydrocarbons[1] and, since then, a large number of investigations have established the importance of coupled heterogeneous–homogeneous reactions in a wide variety of reactions systems, most notably in catalytic combustion,[2-4] partial oxidation of small alkanes,[5-7] and oxidative coupling of methane.[8,9]

All of these reactions systems have very high reaction temperatures ($T > 700$°C) as a common characteristic. Because of these extreme temperatures, noncatalytic (that is, homogeneous) gas-phase reactions can occur in parallel to catalytic surface reactions. For some of the above systems, gas-phase reactions are known to be the product-forming reactions, but in most cases the occurrence of homogeneous reactions is an undesired feature in catalysis because it complicates the fundamental understanding of reaction mechanisms, leads to selectivity losses, and often poses a safety hazard arising from uncontrolled process temperatures, reactor runaway, or even explosive behavior. A well-controlled and safe chemical process requires a good understanding of the underlying reaction mechanisms as well as the main influences of operating parameters on the ignition behavior, and many studies have been dedicated to understanding the ignition of chemical reactions, for both homogeneous and catalytic processes.[10,11]

Catalytic oxidation of hydrogen is an important, yet simple, subset of the above-mentioned hydrocarbon oxidation reactions. The reaction has been studied for many years and is therefore comparatively well understood.[12-15] Beyond its importance as a subset of hydrocarbon oxidations, it is also an

Correspondence concerning this article should be addressed to G. Veser at gveser@pitt.edu.

important oxidation reaction in itself—in rocket propulsion, in lean-burn catalytic combustion, and as a key reaction in fuel cells. The reaction is characterized by particularly wide flammability limits (~3–75 vol % H_2 in air) and very high flame velocities.[10] Its strong exothermicity ($\Delta H \approx -240$ kJ/mol) makes it attractive as a possible energy (heat) source, although the danger of strong explosions restricts its practical application in most cases to highly dilute feed mixtures below the lower flammability limit.

Given that (homogeneous) H_2 oxidation—like the other above-mentioned hydrocarbon oxidation reactions—proceeds by a radical chain-branching mechanism, micromachined reactors offer the potential to tailor the interplay between homogeneous and heterogeneous reaction pathways and thus control homogeneous reactions. Such "microreactors," that is, chemical reactors with characteristic dimensions in the submillimeter range, show a number of advantages over conventional "macroscopic" reactors, which makes them promising tools both for novel chemical process routes and for fundamental studies of chemical reactions.[16-18] Among the advantages of microreactors for chemical processes are their small overall dimensions, small reactant volumes, short pathways for heat and mass transport, and very large surface-to-volume ratios. Because surfaces are known to capture free radicals, the unusually large surface-to-volume ratio in microchannel reactors should influence and ultimately quench homogeneous reactions.

We previously demonstrated that the explosion hazard in H_2 oxidation can indeed be strongly reduced, if not eliminated, through the use of micromachined catalytic reactors.[19-21] We found in experimental investigations that the Pt-catalyzed oxidation of hydrogen with air can be conducted even at stoichiometric conditions without any indication for homogeneous reactions, especially without any explosive behavior, and confirmed in a theoretical study that this behavior is consistent with wall-induced radical quenching. The importance of radical quenching for Pt-catalyzed hydrogen oxidation in "macroscopic" reactors was also demonstrated in simulation studies by Vlachos and coworkers,[22-24] whereas Andrae and Bjoernbom[25] confirmed that chemical (that is, kinetic) wall effects dominate over thermal wall effects, although the latter were found to increase in importance for very fuel lean mixtures.

It is the aim of the present study to gain detailed insights into the interplay between homogeneous and heterogeneous reactions in this reaction system, and in particular to investigate the boundaries for safe reactor operation for hydrogen oxidation in a microchannel reactor. The study is based on detailed numerical simulations with a two-dimensional (2D) boundary-layer model coupled with elementary step kinetics for homogeneous and heterogeneous (Pt-catalyzed) reaction pathways. To completely decouple kinetic quenching effects from thermal effects, we limit our simulations to isothermal conditions. In this way, we evaluate the effect of temperature, pressure, reactor diameter, and fuel-to-air ratio on the interplay between homogeneous and heterogeneous reaction pathways over platinum catalysts, and establish the limits for effective radical quenching in a microchannel reactor.

Model

The reactive flow in the microchannel reactor is described in the present study by means of a 2D boundary-layer model, incorporating balance equations for mass, energy, and momentum.[26] The equations are summarized for an axisymmetric cylindrical coordinate system in Table 1. The CRESLAF routine of the commercially available CHEMKIN software package (version 3.7) is used to solve the resulting 2D partial differential equations (PDEs).[27] These equations are coupled with a detailed description of gas-phase chemistry as well as surface chemistry by CHEMKIN utility packages (CHEMKIN, SURFACE CHEMKIN).

Table 1. Governing Equations of Axisymmetric 2-D Boundary Layer Model

Continuity:

$$\frac{\partial}{\partial z}(\rho u r) + \frac{\partial}{\partial r}(\rho v r) = 0$$

Momentum balance:

$$\rho u \frac{\partial u}{\partial z} \rho v \frac{\partial u}{\partial r} + \frac{\partial p}{\partial z} = \frac{1}{r}\frac{\partial}{\partial r}\left(\mu r \frac{\partial u}{\partial r}\right)$$

Species balance:

$$\rho u \frac{\partial Y_k}{\partial z} + \rho v \frac{\partial Y_k}{\partial r} = \dot{\omega}_k - \frac{1}{r}\frac{\partial}{\partial r}(r \rho Y_k V_{kr}) \qquad (k = 1, \ldots, K_g)$$

Energy balance:

$$\rho u c_p \frac{\partial T}{\partial z} + \rho c_p v \frac{\partial T}{\partial r} = u \frac{\partial p}{\partial z} + \frac{1}{r}\frac{\partial}{\partial r}\left(r\lambda \frac{\partial T}{\partial r}\right) - \sum_{k=1}^{K_g} \dot{\omega}_k W_k h_k - \sum_{k=1}^{K} Y_k V_{k,y} \rho c_{p,k} \frac{\partial T}{\partial r}$$

Equation of state [ideal gas law]:

$$P = \rho R T / \bar{W}$$

Model parameters are chosen to reflect the conditions of our previous experimental studies as closely as possible.[19-21] The inlet linear velocity of the gases is set to 9 m/s (corresponding to Re ≈ 40) with a stoichiometric mixture of hydrogen and air (unless stated otherwise). The microchannel is described as a symmetric tube with the catalyst deposited on the walls. The reactor diameter is varied between 2 mm and 50 μm, and reactor pressure is set to atmospheric pressure unless explicitly stated otherwise. To decouple kinetic effects from thermal effects, we restricted our study to isothermal conditions, varying the temperature between 373 and 2000 K.

A typical simulation took between 1 and 10 min for a single run on a SUN Blade 100 workstation, using between 30 to 100 nonuniformly distributed radial grid points and adaptive stepsizing in the axial direction.

Reaction kinetics

Homogeneous Chemistry. Thermodynamic data, transport properties, and elementary step kinetics for gas-phase chemistry were extracted from the GRI-mechanism 3.0.[28] The resulting kinetics, which incorporates all reactions involving only H- and O-containing species, thus consisting of 9 species and 19 reactions, is summarized in Table 2 (where k_0 is the preexponential factor, E is activation energy, and β is the temperature exponent).

Surface Chemistry

A correct description of the detailed interplay between homogeneous gas-phase reactions and heterogeneous surface re-

Table 2. Gas-Phase Kinetics of H_2–Air Mixture

No.	Reaction	k_0 (mol, cm, s)	β	E (kJ/mol)
1.	$H + O_2 \leftrightarrow O + OH$	5.13×10^{16}	−0.82	69.1
2.	$H_2 + O \leftrightarrow H + OH$	1.8×10^{10}	1.0	37.0
3.	$H_2 + OH \leftrightarrow H_2O + H$	1.2×10^{9}	1.3	15.2
4.	$OH + OH \leftrightarrow H_2O + O$	6.0×10^{8}	1.3	0.0
5.	$H_2 + O_2 \leftrightarrow OH + OH$	1.7×10^{13}	0.0	200.0
6.	$H + OH + M \leftrightarrow H_2O + M^*$	7.5×10^{23}	−2.6	0.0
7.	$O_2 + M \leftrightarrow O + O + M$	1.9×10^{11}	0.5	400.1
8.	$H_2 + M \leftrightarrow H + H + M^{**}$	2.2×10^{12}	0.5	387.7
9.	$H + O_2 + M \leftrightarrow HO_2 + M^{\dagger}$	2.1×10^{18}	−1.0	0.0
10.	$H + O_2 + O_2 \leftrightarrow HO_2 + O_2$	6.7×10^{19}	−1.42	0.0
11.	$H + O_2 + N_2 \leftrightarrow HO_2 + N_2$	6.7×10^{19}	−1.42	0.0
12.	$HO_2 + H \leftrightarrow H_2 + O_2$	2.5×10^{13}	0.0	2.93
13.	$HO_2 + H \leftrightarrow OH + OH$	2.5×10^{14}	0.0	7.9
14.	$HO_2 + O \leftrightarrow OH + O_2$	4.8×10^{13}	0.0	4.2
15.	$HO_2 + OH \leftrightarrow H_2O + O_2$	5.0×10^{13}	0.0	4.2
16.	$HO_2 + HO_2 \leftrightarrow H_2O_2 + O_2$	2.0×10^{12}	0.0	0.0
17.	$H_2O_2 + M \leftrightarrow OH + OH + M$	1.3×10^{17}	0.0	190.5
18.	$H_2O_2 + H \leftrightarrow HO_2 + H_2$	1.7×10^{12}	0.0	15.9
19.	$H_2O_2 + OH \leftrightarrow H_2O + HO_2$	1.0×10^{13}	0.0	7.5

M = third-body enhancement factors:
* H_2O/20.0/.
**H_2O/6.0/ H/2.0/ H_2/3.0/.
†H_2O/21.0/ H_2/3.3/ O_2/0.0/ N_2/0.0/.

actions must consider all reactants and possible reaction intermediates to allow for a description of possible homogeneous–heterogeneous coupling mechanisms. A detailed elementary step mechanism for hydrogen oxidation on platinum is therefore used to describe the kinetics on the catalytically coated wall.[24] The mechanism is summarized in Table 3, where PT(S) indicates a free Pt surface site and species followed by (S) denote adsorbed species. The site density of the Pt surface is set to 2.71E-9 mol/cm^2.[24,25] Because of the isothermal nature of the presented simulations, the simulation results are independent of the thermodynamics of the surface species as long as thermodynamic consistency of the kinetic data is ensured.

Results and Discussion

The focus of the present investigation was on studying the effect of mechanistic interactions between heterogeneous and homogeneous reaction pathways in a catalytic microchannel reactor. Therefore, the simulations are conducted isothermally to focus on kinetic effects rather than (comparatively well studied) thermal effects. Although such isothermicity is next to impossible to realize in a conventional reactor for a strongly exothermic reaction such as hydrogen oxidation, near-isothermal operation can be achieved in appropriately designed microchannel heat-exchange reactors, such as that demonstrated by Schüth and coworkers.[29] Thus, isothermal conditions are not only helpful to develop a scientific understanding of heterogeneous–homogeneous coupling mechanisms, but can also be regarded as realistic in the case of microchannel reactors.

Coupling homogeneous and heterogeneous reaction systems strongly increases the complexity of the overall reaction system. Therefore, to develop a thorough understanding of the heterogeneous–homogeneous reactions, we choose a stepwise approach: we first studied the purely homogeneous ignition as a reference case. The behavior of the purely homogeneous hydrogen oxidation has been thoroughly studied for decades and is therefore well known.[10] This case therefore serves not only as a reference case but also to ensure the reliability of our simulation setup. As a next step, heterogeneous (that is, surface) reactions are introduced, and the fully coupled heterogeneous–homogeneous case is compared to the homogeneous reference case as well as a purely heterogeneous case. Finally, the influence of some of the main process parameters is studied (reactor diameter, pressure) and critical conditions for safe reactor operation based on radical quenching were deduced from the results. The results are presented and discussed in detail in the following.

Inert wall (homogeneous reaction)

The ignition behavior of a stoichiometric H_2–air mixture (H_2:O_2 = 2:1) in an isothermal microreactor with an inert wall, that is, a purely homogeneous reaction system, is studied as the reference case. The channel diameter is set to 1 mm and gas mixtures are fed with 9 m/s linear velocity according to the experiment.

The results are shown in Figure 1 where the ignition distance X_{ign} is plotted as a function of reactor temperature. We define ignition distance as the distance from the reactor entrance to the point where 50% conversion of H_2 is reached at the centerline of the reactor. The ignition curve shows the well-known behavior of gas-phase hydrogen (and hydrocarbon) combustion reactions: the ignition distance strongly increases with decreasing reaction temperature and eventually shows an asymptotic behavior toward a critical ignition temperature, which is about 930 K in our case. Below this critical temperature, ignition can no longer occur for any reactor length.

This behavior agrees well with the well-known (temporal) ignition delay in H_2 oxidation, which has been studied for many decades.[10] Ignition of the gas-phase reaction requires the buildup of a "radical pool," that is, a critical concentration of highly reactive radicals, until the net chain-branching factor increases beyond unity and a fast self-acceleration of the radical chain mechanism leads to ignition. This initial formation of radicals follows the usual Arrhenius rate expression and thus shows an exponential dependency on temperature, which is reflected in the shape of the ignition curve. At lower temperatures, ignition therefore occurs with increasing (temporal) delay, which translates into an increasing spatial ignition delay

Table 3. Surface Reaction Steps and Rate Parameters*

No.	Reaction	s	k_0 (1/s)	$E_{des/act}$ (kJ/mol)
1.	$H_2 + 2PT(S) \Rightarrow 2H(S)$	0.48		0.0
2.	$2H(S) \Rightarrow H_2 + 2PT(S)$		9.4E+11	84.0
3.	$O_2 + PT(S) \Rightarrow O_2(S)$	0.03		0.0
4.	$O_2(S) \Rightarrow O_2 + PT(S)$		1.0E+13	214.2
5.	$OH + PT(S) \Rightarrow OH(S)$	1.00		0.0
6.	$OH(S) \Rightarrow OH + PT(S)$		1.0E+13	264.6
7.	$H_2O + PT(S) \Rightarrow H_2O(S)$	0.75		0.0
8.	$H_2O(S) \Rightarrow H_2O + PT(S)$		1.0E+13	42.0
9.	$H + PT(S) \Rightarrow H(S)$	1.00		0.0
10.	$H(S) \Rightarrow H + PT(S)$		1.0E+13	252.84
11.	$O + PT(S) \Rightarrow O(S)$	1.00		0.0
12.	$O(S) \Rightarrow O + PT(S)$		1.0E+13	281.4
13.	$OH(S) + PT(S) \Rightarrow O(S) + H(S)$		6.1E+11	102.48
14.	$H(S) + O(S) \Rightarrow OH(S) + PT(S)$		1.7E+10	50.82
15.	$H_2O(S) + PT(S) \Rightarrow H(S) + OH(S)$		1.2E+10	77.28
16.	$H(S) + OH(S) \Rightarrow H_2O(S) + PT(S)$		3.5E+11	52.08
17.	$H_2O(S) + O(S) \Rightarrow 2OH(S)$		1.0E+11	52.92
18.	$2OH(S) \Rightarrow H_2O(S) + O(S)$		1.0E+11	79.38

*From Aghalayam et al.[24]

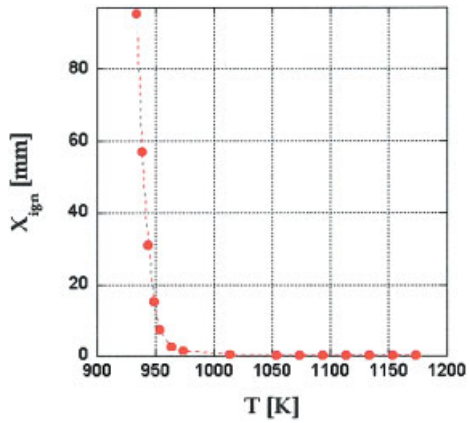

Figure 1. Ignition distance vs. reaction temperature in a microchannel reactor (diameter: 1 mm) and an inert wall, that is, purely homogeneous reactions.

See main text for definition of ignition distance and parameters of the simulation. [Color figure can be viewed in the online issue, which is available at www.interscience.wiley.com.]

in a tubular flow reactor ($x_{ign} = vt_{ign}$, where x_{ign} is the ignition distance, v is the flow velocity of the gases, and t_{ign} is the temporal ignition delay). At sufficiently low temperatures, radical recombination reactions balance radical initiation reactions and thus eventually lead to a suppression of homogeneous ignition.

Catalytic wall (platinum)

Next, the ignition of H_2/air mixtures in a catalytically coated microchannel reactor is studied and compared to the purely homogeneous case. Pt is chosen as catalyst for several reasons: First, it is a well known and widely used catalyst for oxidation reactions and is therefore of practical relevance. Furthermore, Pt was used in our experimental investigations and therefore allows comparison between simulation and experimental results.[20,21] Finally, the kinetics of H_2 oxidation on Pt has been extensively studied in the past and the available reaction kinetics are therefore comparatively well tested and reliable.[14,23-25,30-32]

Results are shown in Figure 2, where results for the fully coupled heterogeneous–homogeneous reaction system in a Pt-coated microchannel reactor (filled squares and solid line) are shown compared with the purely homogeneous gas-phase ignition (circles and dashed line) and the purely catalytic ignition (that is, no homogeneous reactions; open squares and dotted line).

Clearly, the coupled heterogeneous–homogeneous case shows a completely different ignition behavior from that of the purely homogeneous case: for $T < 1000$ K, ignition distances for the catalytic cases are strongly reduced compared to the purely homogeneous case, given that neither catalytic case shows the asymptotic approach of the homogeneous ignition toward a lower critical temperature, but displays ignition down to the lowest temperatures studied ($T = 373$ K). Even though catalytic ignition occurred for even lower temperatures, this was not studied any further because the Pt surface kinetics have not been verified for that temperature range, and the possible condensation of the reaction product (water) must be taken into account for a correct description of the reaction as well as the flow in the microreactor channel in this temperature range.

The strongly reduced ignition distance—and particularly the occurrence of ignition for much lower temperatures—is expected upon addition of a catalyst. The catalyst opens new reaction pathways with lower activation energy, accelerating reactions at higher temperatures and extending the range of reactivity toward lower temperatures. It is well known that hydrogen oxidation occurs over Pt catalysts at temperatures as low as room temperature even for very dilute H_2/air mixtures, an effect that can be used in the start-up of catalytic reactors.[33,34] Comparison with the ignition curve for the (theoretical) case of a purely catalytic reaction system (that is, a system in which the homogeneous reactions have been artificially "switched off"; open squares and dotted line in Figure 2) confirms that the two cases show identical ignition distances in this temperature range, that is, this branch of the fully coupled ignition curve is completely dominated by surface reactions.

This behavior changes at $T > 1000$ K: the ignition curve for the fully coupled case crosses the ignition curve for the purely homogeneous case and shows a sudden bend toward shorter ignition distances, deviating from behavior of the purely catalytic case. In this high-temperature range, ignition distances for the coupled case fall between the purely homogenous and the purely catalytic case, indicating that neither of the individual reaction pathways suffices to describe the coupled heterogeneous–homogeneous case. The deviation from the ignition behavior of the purely catalytic case indicates that, at these high temperatures, homogeneous reactions start to influence the ignition behavior. In fact, the parallel trends between the

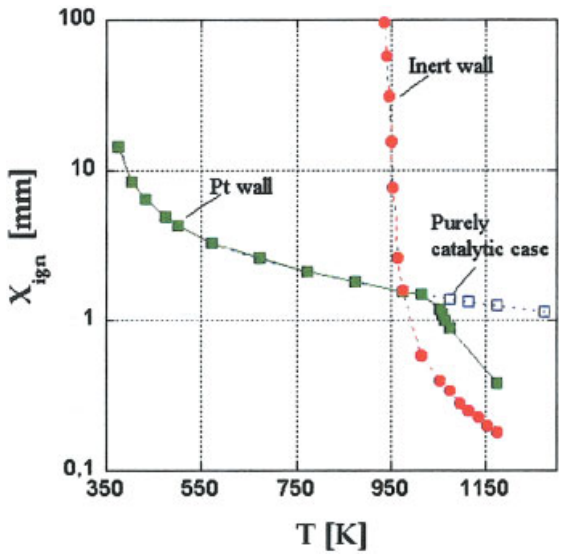

Figure 2. Ignition distance vs. reaction temperature for a reactor (diameter: 1 mm) and inert wall (purely homogeneous reactions, filled circles), Pt-coated catalytic wall (full heterogeneous–homogeneous coupled case, filled squares), and a catalytic wall without gas-phase reactions (purely heterogeneous case, open squares).

[Color figure can be viewed in the online issue, which is available at www.interscience.wiley.com.]

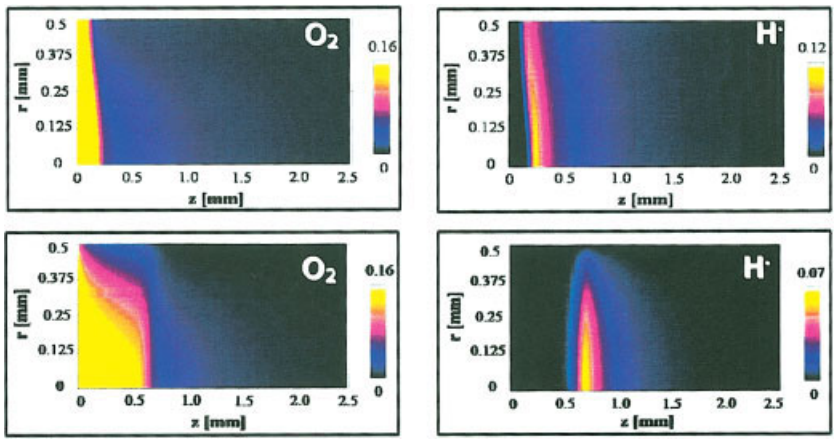

Figure 3. Contour plots of O_2 concentration (left column) and H radical concentration (right column) for an inert reactor channel (top row) and a Pt-coated reactor channel (bottom row) (diameter: 1 mm) as a function of axial (z) and radial (r) distances at $T = 1113$K.

The reactor wall is at the top of the graphs, whereas the symmetry line of the tubular channel is at the bottom ($r = 0$ mm). Flow direction is from left to right. [Color figure can be viewed in the online issue, which is available at www.interscience.wiley.com.]

purely homogeneous ignition curve and the ignition curve for the fully coupled case even suggest that homogeneous reactions are qualitatively dominating the ignition, although a substantial off-set in ignition distance is observed arising from the presence of the surface reactions. Interestingly, this off-set is toward *longer* ignition distances, that is, the presence of the catalyst leads to an additional ignition *delay* rather than the acceleration of ignition as one might expect and as observed for temperatures < 1000 K. Overall, the simulations thus show that the catalyst acts as an ignition *promoter* at low temperatures and as ignition *inhibitor* at sufficiently high temperatures.

The reason for the ignition-impeding behavior of the catalyst at high reaction temperatures can be seen in the concentration contour plots shown in Figure 3. Concentration profiles of molecular oxygen and hydrogen radicals in the gas phase are shown for the upper half of a reactor with 1 mm diameter at $T = 1113$ K. Gas flow is from left to right, the reactor wall is at the top of the graphs, and the symmetry line of the channel is at the bottom.

The oxygen concentrations show two striking differences between the inert wall (top row) and the Pt wall (bottom row): for the Pt wall (that is, the fully coupled case) ignition at the wall occurs almost instantaneously, whereas ignition at the centerline is strongly delayed compared with the inert case. Clearly, in the Pt-coated reactor, the reaction starts heterogeneously, that is, on the catalyst surface, near the reactor entrance, and ignition of the bulk gas phase occurs with a significant spatial delay at $z \approx 0.6$ mm.

The fast catalytic consumption of O_2 near the wall is not surprising, considering that catalysts are being used in catalytic combustion precisely for the purpose of facilitating ignition. The reason for the delayed ignition at the centerline can be found in the H-radical concentration plots, given that H-radicals are a sensitive indicator for the occurrence of homogeneous gas-phase reactions. The H-radical concentrations show the same delayed ignition at the centerline as observed in the oxygen concentrations. However, the maximum H-radical concentration is only about 7 mol % in the fully coupled case vs. 12 mol % in the purely homogeneous case. This indicates that the homogeneous reaction has been weakened by the presence of the catalytic wall. Furthermore, the H-radical concentration drops to zero in the boundary layer above the catalytic wall, suggesting that the Pt surface acts as a strong radical scavenger. Apparently, the reactant depletion in the boundary layer and radical scavenging by the surface reaction strongly weaken the homogeneous reactions and thus delay ignition of the (bulk) homogeneous ignition.[35]

Given that this effect can be expected to become more dominant as the reactor diameter decreases (and thus the surface-to-volume ratio increases), the effect of decreasing the reactor diameter into the micrometer range was studied next.

Influence of some of the main process parameters

Effect of Microdimensions. The effect of decreasing diameters of a Pt-coated microchannel reactor is shown in Figure 4. Ignition distance is shown vs. temperature for reactor diameters of 2 mm, 1 mm, 500 μm, 300 μm, 250 μm, 100 μm, and 50 μm, corresponding to surface-to-volume ratios between 2000 and 80,000 m^{-1}.

The ignition curves fall essentially into two groups: the four ignition curves for diameters of 2 mm to 300 μm, and the three curves for diameters of 250, 100, and 50 μm. The curves at larger channel diameters ($d \geq 300$ μm) show qualitatively the same behavior as described in the preceding section, that is, they show two distinct branches for higher and lower temperatures, respectively. The high-temperature ignition shows very little dependency on channel diameters, with only a minor increase of ignition distance with decreasing diameter. This confirms the earlier interpretation of this ignition regime as largely homogeneously dominated with the surface reaction adding a delaying effect only on the (homogeneous) ignition.

In contrast to that, the low-temperature branch shows a strong decrease in ignition distance with decreasing channel diameters. This dependency of the ignition delay seems surprising in light of our previous interpretation of this ignition branch as purely catalytic (see previous section): if the ignition is a pure surface reaction, the reactor diameter should not have

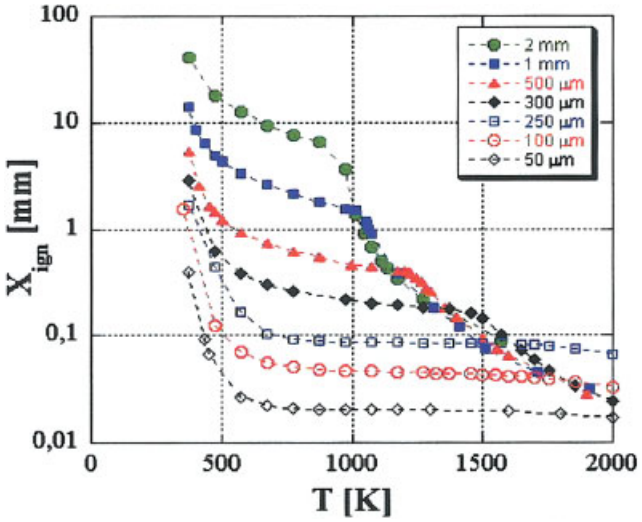

Figure 4. Ignition distance vs. reaction temperature for a reactor with catalytic Pt-wall varying channel diameters (2 mm to 50 μm).

[Color figure can be viewed in the online issue, which is available at www.interscience.wiley.com.]

any significant impact on ignition. This apparent contradiction is caused by our definition of ignition as the point of 50% hydrogen conversion *at the centerline* of the flow channel. As a result of this definition, we are in this case not observing the ignition process directly, but rather observe the catalytic wall ignition delayed by the diffusive transport from the centerline to the wall. Because the length of this diffusion path increases with increasing channel diameter, the transport process takes correspondingly longer, leading to an increasing (apparent) spatial ignition delay. This delay is further increased by the changing surface-to-volume ratio: because catalytic reaction rates scale with the surface area (that is, with r) and gas-phase concentrations scale with the reactor volume (that is, with r^2), with increasing reactor diameter the surface reaction will take longer to deplete the gas phase sufficiently to observe a 50% drop in H_2 concentration.

Additionally, one observes in Figure 4 a continuous shift in the transition point from the catalytically dominated to the homogeneously dominated ignition branch (that is, the sudden bend in the curve) toward higher temperatures with decreasing reactor diameter. This shift is again an effect of the changing surface-to-volume ratio of the microchannel: the relative rate of surface reaction vs. homogeneous gas-phase reaction increases with increasing surface-to-volume ratio. Thus, with decreasing microchannel diameter, the catalytic reaction continues to dominate the overall ignition behavior up to higher reaction temperatures.

Although the transition from heterogeneously dominated to homogeneously dominated ignition progressed gradually for d values from 2 mm to 300 μm, a qualitative change in the ignition behavior occurs between d values of 300 and 250 μm, that is, in the transition to the second group of ignition curves: For smaller microchannel diameters ($d < 300$ μm), only one ignition branch is observed up to the maximum reactor temperature of $T = 2000$ K. (Even higher temperatures were not studied because the validity of the reaction kinetics as well as the practical relevance of simulations at such extreme temperatures become questionable.)

To better understand the absence of the homogeneous ignition branch for $d < 300$ μm, Figure 5 shows the contour plots for oxygen and hydrogen radical concentrations in three microchannel reactors with diameters of 1 mm, 500 μm, and 300 μm at $T = 1113$ K. The catalytic wall is at the top of the graphs and the symmetry line of the reactor channel is at the bottom. (Note that for the sake of better visibility the y-axes are not drawn to scale in these plots.) One can see that the sharp transition from catalytic ignition at the reactor wall to homogeneous ignition in the bulk of the gas phase (as explained

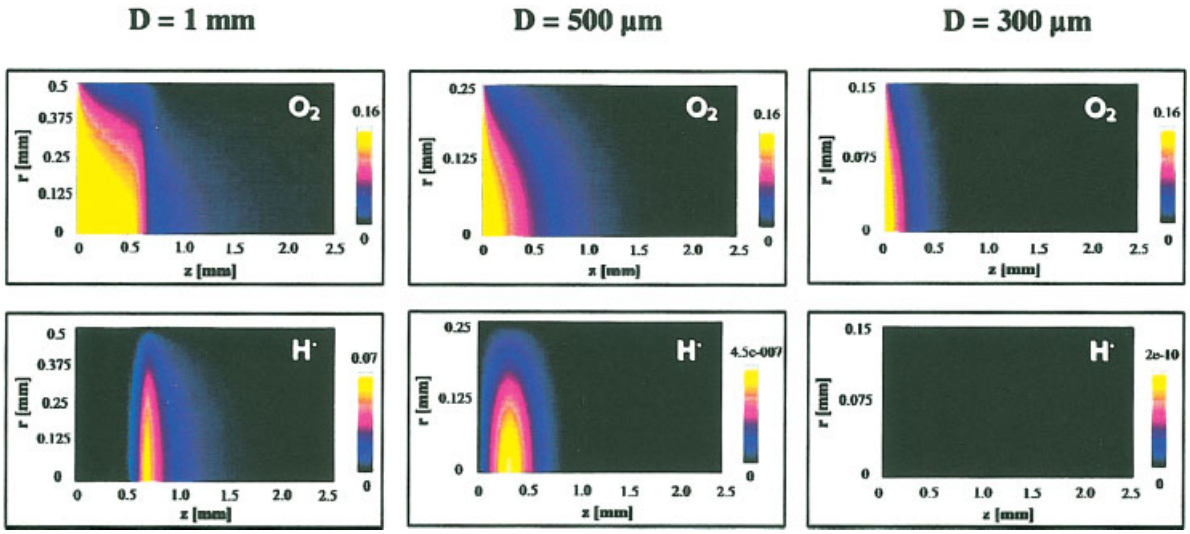

Figure 5. Contour plot of O_2 concentration (top row) and H radical concentration (bottom row) as a function of axial (z) and radial (r) direction for a Pt-coated microchannel with diameters of 1 mm (left), 500 μm (middle), and 300 μm (right) at $T = 1113$ K.

[Color figure can be viewed in the online issue, which is available at www.interscience.wiley.com.]

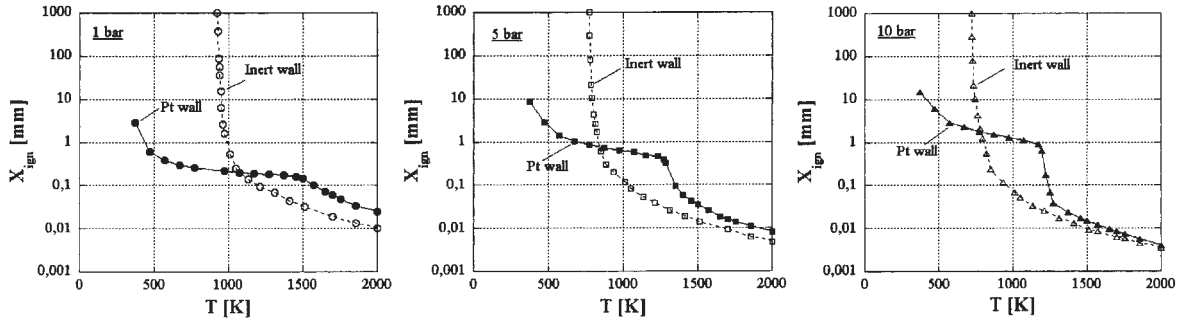

Figure 6. Ignition distance vs. reaction temperature for a microchannel (diameter: 300 μm) at 1 bar (left), 5 bar (middle), and 10 bar (right).

Filled symbols represent the full heterogeneous–homogeneous coupled case (Pt-coated walls), whereas open symbols represent the purely homogeneous case (inert walls).

above; see also Figure 3) becomes very much "smeared out" for the 500-μm channel. Correspondingly, the maximum in the H-radical concentration also broadens significantly and decreases by more than four orders of magnitude. Both effects indicate a severe weakening of homogeneous reactions for this reactor diameter and temperature. Figure 4 shows that for the 500-μm microchannel, this reactor temperature lies in the transition region from heterogeneously dominated to homogeneously dominated ignition behavior, which is thus consistent with the current observation.

For the microchannel with $d = 300$ μm, oxygen consumption is strongly accelerated and H-radical concentrations drop below the numerical accuracy of our simulations ($\sim 10^{-10}$ mol %). This indicates that for this diameter oxygen consumption is fast because of the very short transport pathways and, most important, homogeneous reactions are completely quenched. These results thus confirm our previous experimental and mechanistic observations that a Pt-coated microchannel reactor can indeed lead to complete quenching of homogeneous reactions. The critical transition occurs (for stoichiometric hydrogen/air mixtures and Pt-coated walls) at d values between 300 and 250 μm, which is in good qualitative agreement with our previous experimental investigations, where we observed homogeneous ignition for $d = 2$ mm, but did not see homogeneous (that is, explosive) behavior in a 120-μm annular reactor.[21]

Influence of Reaction Pressure. It is well known that increasing pressure accelerates homogeneous reactions because reactant density—and thus the mean free path or the frequency of intermolecular collision—increases with pressure. Therefore, the influence of reactor pressure on the interplay between homogeneous and heterogeneous reactions and on the overall ignition behavior of catalytic hydrogen oxidation in the Pt-coated microchannel reactor was studied next. Homogeneous reactions typically scale with the square of the reactor pressure (as a result of the dominance of bimolecular reaction steps), whereas surface reactions tend to scale approximately linearly with pressure because the only pressure-dependent steps are adsorption steps, which are usually first order in the partial pressure of the reactant. It can thus be expected that the interplay between homogeneous and heterogeneous reactions is strongly affected by reactor pressure and the observed kinetic quenching—and thus microreactor safety—needs to be reevaluated for different pressure conditions.

Figure 6 shows the ignition distance for a stoichiometric H_2–air mixture in a 300-μm microchannel reactor as a function of temperature for a reactor pressure of 1 bar (circles), 5 bar (squares), and 10 bar (triangles). Results for a Pt-coated microchannel, that is, the coupled homogeneous–heterogeneous case (filled symbols and solid lines), are shown in comparison with a microchannel with inert walls, that is, the purely homogeneous case (open symbols and dashed lines), which corresponds to the purely homogeneous reference case.

One can see that the ignition curves for both cases show qualitatively identical behavior at all three pressures. For the purely homogeneous case, it is characterized by the above-described continuous increase in ignition distance with decreasing temperature, asymptotically approaching a critical limit temperature below which ignition no longer occurs. For the coupled homogeneous–heterogeneous case, the curves show the two distinct ignition branches, of which the steeper, high-temperature branch is dominated by the ignition of the homogeneous gas-phase reaction, and the flat, low-temperature branch is dominated by the ignition of the catalytic surface reaction, as described in detail earlier for the ambient pressure case in the Catalytic wall section.

With increasing pressure, the ignition distance for both the purely homogeneous case and the homogeneously dominated high-temperature branch of the fully coupled case shift toward lower temperatures and shorter ignition distances. This is explained by the increasing density of the gas phase, which increases the frequency of intermolecular collisions and thus the frequency of reactive events. However, this decrease in ignition distance is more pronounced for the coupled case than for the purely homogeneous case, which results in a closing of the gap between the ignition curves for the two cases. The gap is very pronounced at 1 bar and has almost completely disappeared at 10 bar. Given that the delayed ignition in the coupled case arises from the influence of the catalytic surface reaction on the homogeneously dominated ignition, this indicates that with increasing pressure the overall reaction is increasingly determined by homogeneous gas-phase reactions, as expected, because of the different pressure dependencies of the homogeneous vs. heterogeneous reaction pathways (explained in the introduction to this section).

Additionally, one can see in Figure 6 that the ignition distance for the heterogeneously dominated branch of the coupled case *increases* with increasing pressure. For an easier direct

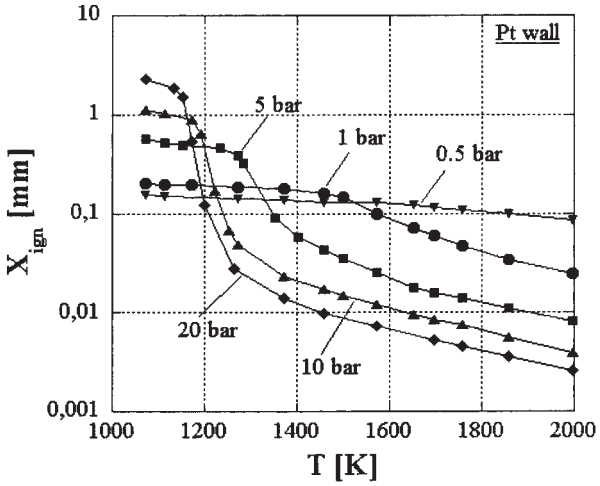

Figure 7. Ignition distance vs. reaction temperature for a Pt-coated microchannel (diameter: 300 μm) at 0.5 bar (downward triangles), 1 bar (circles), 5 bar (squares), 10 bar (upward triangles), and 20 bar (diamonds).

comparison, the ignition curves for only the coupled case are shown again in Figure 7 for a temperature range of 1000–2000 K. Two more ignition curves for reactor pressures of 0.5 and 20 bar, respectively, are added for completeness. One can clearly see that with increasing pressure the high-temperature ignition branches shift toward shorter ignition distances, whereas the low-temperature branches shift in the opposite direction. As a consequence, the transition between the two branches becomes increasingly gradual with decreasing pressure and the transition point shifts toward higher temperatures, until, at $P = 0.5$ bar, the transition has almost disappeared.

The opposing effect of pressure on the two different ignition branches for the coupled heterogeneous–homogeneous case can again be understood based on the concentration profiles inside the microchannel. Figure 8 shows contour plots of oxygen concentrations in the upper half of the Pt-coated microchannel at an intermediate temperature of 1253 K and reactor pressures of 1 bar (left), 5 bar (middle), and 10 bar (right), respectively. The ignition at this temperature is purely catalytic at 1 bar, strongly homogeneously dominated at 10 bar, and right in the transition region between these two cases for 5 bar (see Figure 7). In agreement with this, oxygen is consumed gradually across the microreactor cross section at 1 bar, whereas at 5 bar oxygen consumption near the catalytic wall still appears gradual but the remaining oxygen near the centerline of the reaction channel is consumed almost instantaneously at $z \approx 0.05$ cm, and a similar behavior is observed at 10 bar, compressed onto an axial scale of $z \approx 0-0.02$ cm.

The smooth concentration profile at 1 bar reflects the previously discussed effect of oxygen consumption arising from a purely catalytic wall reaction and subsequent consumption of oxygen in the bulk fluid phase by diffusive transport. With increasing pressure, diffusion is slowed down (given that $D \propto P^{-1}$), whereas at the same time heterogeneous and homogeneous reactions are accelerated. Because the surface reaction is mass transfer limited, increasing pressure has no significant effect on this reaction pathway. Homogeneous ignition, on the other hand, is strongly accelerated and thus consumes the remaining oxygen after a short ignition delay, thus giving rise to the steep oxygen gradients at 5 and 10 bar. The decreasing ignition delay with increasing pressure thus indicates that homogeneous ignition—although still trailing the virtually instantaneous surface ignition—becomes increasingly dominant with increasing pressure.

At lower temperatures, this picture changes significantly. Figure 9 shows oxygen concentration profiles at 1, 5, and 10 bar for a temperature of $T = 1113$ K, which corresponds to the low-temperature branch for all three pressures. A smooth, gradual consumption of oxygen across the microreactor cross section is observed at all three pressures. However, although the initial consumption of oxygen near the catalytic wall is accelerated with increasing pressure, the consumption in the bulk phase now appears delayed, giving rise to an increasingly spread-out concentration profile. This again reflects the purely catalytic nature of the reaction at this comparatively low temperature. Increasing pressure enhances the rate of reactant adsorption and thus accelerates the initial rate of catalytic reaction, explaining the faster oxygen consumption near the catalytic wall. However, after initial consumption of the reactants in the boundary layer above the wall, diffusive mass transfer becomes limiting for the surface reaction. The inverse dependency of gas-phase diffusion on pressure ($D \propto P^{-1}$) therefore leads to slower oxygen consumption at the centerline of the reactor with increasing pressure.

Overall, the two opposing effects of increasing homogeneous reaction rate and decreasing rate of diffusion with increasing pressure thus explain the diverging behavior of the ignition curve for the coupled heterogeneous–homogenous case at high- and low-temperature conditions, respectively.

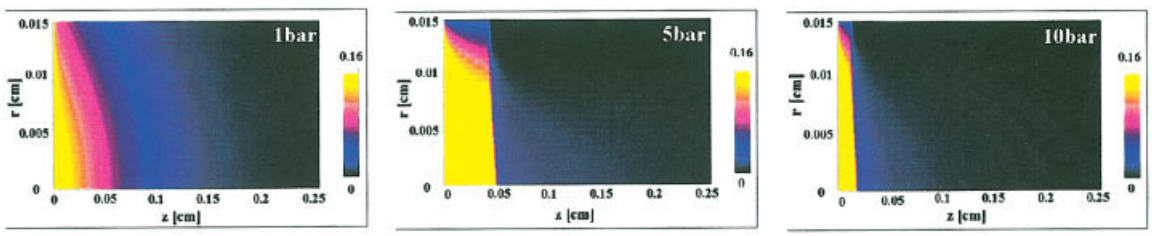

Figure 8. Contour plot of O_2 concentration in a Pt-coated microchannel reactor (diameter: 300 μm) at $T = 1253$ K and $P = 1$ bar (left), 5 bar (middle), and 10 bar (right), respectively.

[Color figure can be viewed in the online issue, which is available at www.interscience.wiley.com.]

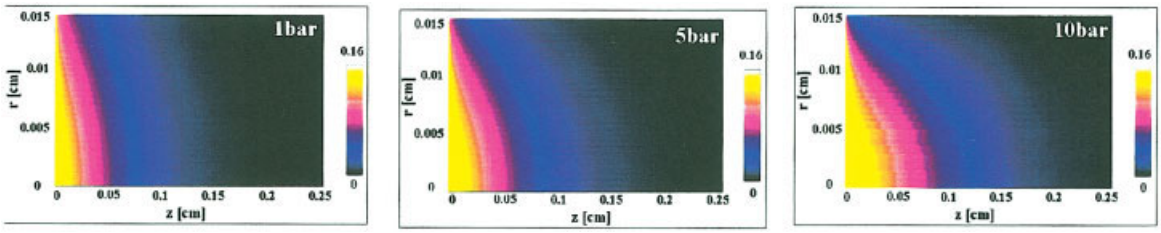

Figure 9. Contour plot of O_2 concentration in a Pt-coated microchannel reactor (diameter: 300 μm) at T = 1113 K and P = 1 bar (left), 5 bar (middle), and 10 bar (right), respectively.

[Color figure can be viewed in the online issue, which is available at www.interscience.wiley.com.]

Critical conditions for safe reactor operation

Determination of Critical Parameters. Given the strong dependency of the quenching of homogeneous reactions on pressure, it seems useful to develop a mathematical expression that allows an exact determination of the critical parameters (pressure, temperature, microchannel diameter) without having to repeat detailed numerical simulations for each case. To this purpose, we used a mathematical fit for the ignition distance (X_{ign}) data vs. temperature (T) for the coupled homogeneous–heterogeneous case. The two ignition branches (low-T heterogeneous and high-T homogeneous ignition) were fitted separately for different reactor diameters (D) and reaction pressures (P) as shown schematically in Figure 10. An Arrhenius-type expression was used: $X_{ign} = \{a \exp[b/(T - c)] + d\}$, where all parameters have well-defined physical meanings: $(a + d)$ is a critical ignition distance X_c, that is, the minimal, asymptotic ignition distance for $T \rightarrow \infty$; c is the critical ignition temperature, that is, the temperature below which no homogeneous ignition can occur; and b is the apparent activation energy of the ignition process divided by the universal gas constant ($b = E_{app}/R$).

Figure 11 shows the critical ignition distance X_c vs. pressure and microchannel diameter for the homogeneous ignition branch (uniform black surface) and the heterogeneous ignition branch (grayscale surface). One can see that for high pressure and large channel diameters the critical ignition distance for the homogeneous branch becomes much shorter than that for the heterogeneous ignition branch, whereas for lower pressures and small microchannel diameters the critical heterogeneous ignition distance drops below that of the homogeneous one. The resulting intersecting line between these two surfaces therefore delimits the parameter range for "intrinsically" safe reactor operation: once the critical ignition distance for heterogeneous ignition process drops below the critical ignition distance for homogeneous ignition, the homogeneous reaction is completely quenched, that is, ignition of the homogeneous reaction can no longer occur, *independent of reaction temperature*.

A close mathematical fit for the dependency of the critical microchannel diameter on pressure along the intersecting line between the two ignition surfaces was obtained with the following expression (see Figure 12): $d_c/[\mu m] = 4.61 \times 10^{-9} \exp[-(P/[bar] - 99.97)/3.632] - 295$. From this, the

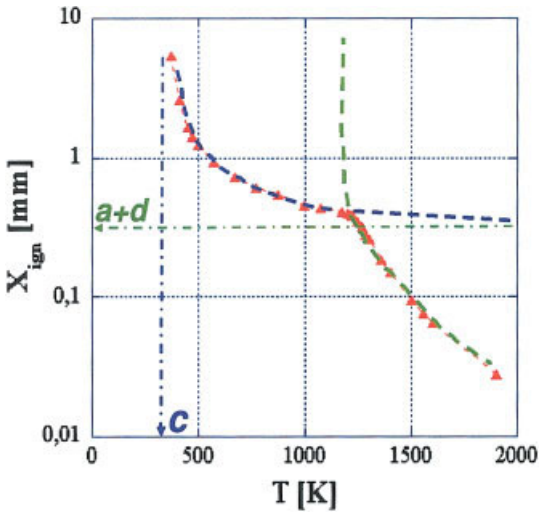

Figure 10. Schematic illustrating the mathematical fitting of a general expression of the form $X_{ign} = \{a \exp[b/(T - c)] + d\}$ to the two ignition branches of the coupled heterogeneous–homogeneous case.

All fit parameters have clearly defined physical meanings: $(a + d)$ is the critical ignition distance, b is the apparent activation energy, and c is the critical ignition temperature. [Color figure can be viewed in the online issue, which is available at www.interscience.wiley.com.]

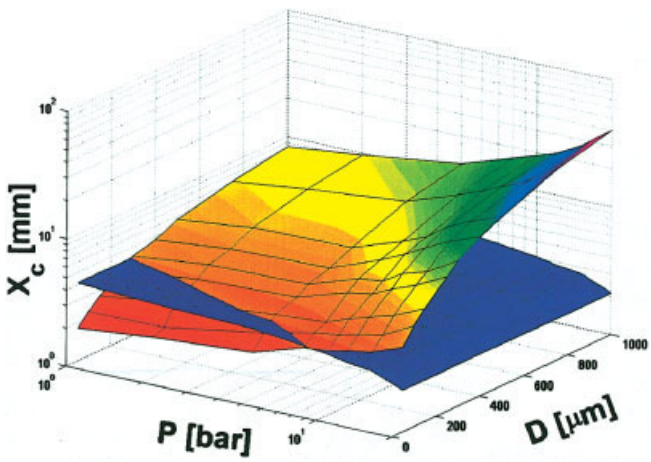

Figure 11. 3D plot of critical ignition distance (X_c) vs. reactor pressure (P) and reactor diameter (D) for H_2 oxidation in a Pt-coated microchannel reactor.

[Color figure can be viewed in the online issue, which is available at www.interscience.wiley.com.]

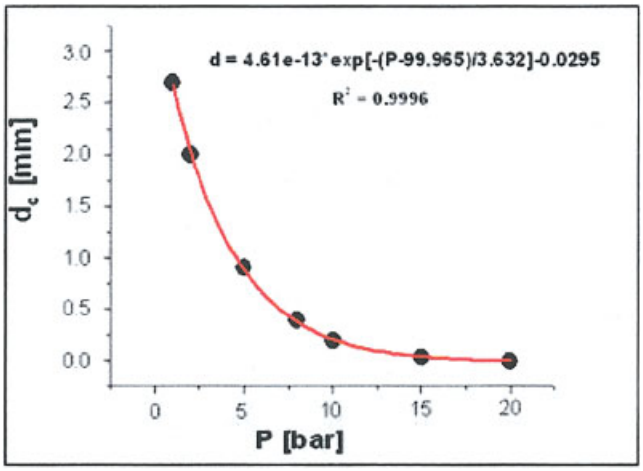

Figure 12. Critical diameter (d_c) vs. reactor pressure along the intersecting line of the two ignition surfaces in Figure 11.

[Color figure can be viewed in the online issue, which is available at www.interscience.wiley.com.]

values of two critical parameters of practical importance can be determined. On the one hand, the critical diameter below which homogeneous reactions can no longer occur can be calculated. At atmospheric pressure, this diameter is 285 μm. On the other hand, this expression also allows calculation of the critical pressure above which no microchannel diameter exists any longer for which complete quenching of homogeneous ignition can be attained. This critical pressure is $P = 9.4$ bar; that is, for pressures in excess of 9.4 bar the "intrinsic" reactor safety breaks down for the current reaction system.

These calculations thus demonstrate the bounds of safe microreactor operation for a stoichiometric H_2–air system. They also generally indicate that for catalytic microreactors, the influence of high-pressure conditions needs to be reevaluated in detail for each specific reaction system.

Mechanistic Study of Ignition Mechanism. As described above, the mathematical fit of the ignition curves also yields an apparent activation energy for the ignition process, and therefore can yield insights into the ignition mechanism for the two different reaction pathways. The calculated apparent activation energy ($E_{app} = bR$, where R is the ideal gas constant) of the homogeneous branch is 201 kJ/mol. This value agrees well with the activation energy for OH formation from H_2 and O_2 in the gas-phase mechanism (reaction 5 in Table 2), indicating that this reaction step is the rate-determining step in homogeneous ignition. This is also confirmed by a reaction path analysis for the homogeneous reaction steps.

Interestingly, this differs from the typically reported limiting reaction for chain branching in hydrogen oxidation: most previous studies,[10] including very detailed recent results,[36] found OH formation from O_2 and H to be the rate-limiting step (reaction 1 in Table 2). We saw above that the presence of the Pt wall leads to an additional ignition delay for the high-temperature, homogeneously dominated ignition branch, which was explained by the radical capturing of the catalytic surface. Apparently, this radical capturing reduces the radical concentrations in the gas phase sufficiently to reduce the importance of the radical-mediated ignition steps and make the formation of radicals from the molecular reactants H_2 and O_2 the dominating reaction step upon ignition. The coupling between the heterogeneous and homogeneous reaction pathways thus not only leads to quenching of homogeneous reactions for sufficiently small channel diameters, but also changes the ignition mechanism for diameters at which homogeneous ignition is still possible and dominant.

An equivalent mathematical fit for the heterogeneously dominated (low-temperature) ignition branch yields an apparent activation energy of 53.4 kJ/ mol. In this case, the Pt mechanism does not allow identification of a single reaction step with this activation energy, but rather shows three reaction steps (reactions 14, 16, and 17 in Table 3) with activation energies in sufficiently close agreement with this value. These steps describe the catalytic formation of OH from H and O (step 14), the formation of H_2O from H and OH (step 16), and the formation of OH from H_2O and O (step 17). Although the third step seems unlikely to be rate determining for the ignition process (because it involves the decomposition of the reaction product), both of the first two reaction steps are reasonable candidates for a rate-limiting ignition step.

To further distinguish the importance of these reaction steps, net reaction rates for all nine surface reactions along the whole reactor length are calculated. Figure 13 shows the local net rate of the individual surface reaction steps at $T = 1113$ K (that is, for the heterogeneously dominated branch) vs. reactor length along with the integral hydrogen conversion vs. reactor length (secondary y-axis). The result shows that reaction 14 [that is, the formation of OH(s) from O(S) and H(S)] not only is one of the two slowest reaction steps in the reaction system, but also is the only reaction step that shows a strong sensitivity to the ignition step, as indicated by the sharp maximum in reaction rate localized in the area where the conversion shows the sharp initial increase. In contrast to that, reactions 16 and 17 not only show net reaction rates that are orders of magnitude larger, but also display no particular sensitivity to ignition. Thus, we can identify the formation of OH from O and H on the Pt surface as the ignition-determining step for the heterogeneously dominated, low-temperature branch.

It should be mentioned that this result is in disagreement with previous studies, which identified adsorption and desorption of hydrogen on the Pt surface,[37] or reaction 16, that is, water formation from OH(S) and H(S) on the catalyst surface,[38] respectively, as rate-determining steps. We cannot completely resolve this discrepancy between our findings and the findings of these studies (nor the discrepancy between their findings), but a significant difference between these previous studies and our present study is the fact that we restricted our investigation to isothermal surface conditions. Therefore, the temperature increase upon ignition in the previous studies might lead to a strong increase in the backward reaction OH(S) + PT(S) $\Rightarrow$ O(S) + H(S) (reaction 13 in Table 3) because this reaction has a particularly large activation energy. This could open a competition for OH(S) between this backward reaction and water formation by reaction 16, thus introducing sensitivity toward the latter reaction and reconciling our findings with the results from Ikeda et al.[38] Another difference from Rinnemo et al.[37] is the high nitrogen dilution and low-temperature range (~300–500 K) of their investigation. Nevertheless, their observation that the Pt surface is essentially H-poisoned up to the ignition point agrees qualitatively well with the surface coverages ob-

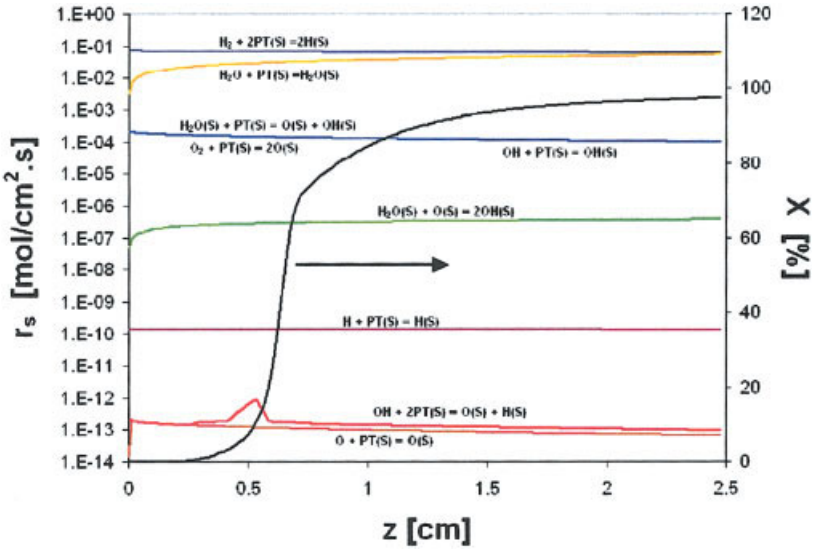

Figure 13. Net surface reaction rate (r_s) of the nine reversible reactions on the Pt surface as well as integral conversion (X, right-hand y-axis) vs. reactor length (z) in a Pt-coated microchannel reactor (diameter: 300 μm) at T = 1113 K.

The lines are labeled with the respective reaction equation. [Color figure can be viewed in the online issue, which is available at www.interscience.wiley.com.]

served in our simulations. However, this H-coverage is more likely to become a rate-limiting catalyst poison in their low-temperature regime than at the significantly higher temperatures that we focus on in our study.

Influence of Equivalence Ratio. It is well known that the fuel-to-oxygen ratio in the reactor feed has a strong influence on the ignition behavior.[10] We therefore conducted a brief investigation of the influence of the fuel-to-air ratio on the above-discussed observations in the heterogeneous–homogeneous ignition of H_2/air mixtures.

Figure 14 shows the results from simulations of H_2/air mixtures in a Pt-coated microchannel with 300 μm diameter for different H_2/air mixtures. The hydrogen-to-air ratio is denoted by the equivalence ratio ϕ, which is defined as usual as $\phi = (n_{\text{fuel}}/n_{\text{oxygen}})/(n_{\text{fuel}}/n_{\text{oxygen}})_{\text{stoich}}$, that is, it denotes the molar fuel-to-oxygen ratio divided by the fuel-to-oxygen ratio at the stoichiometric point for total oxidation. Thus, $\phi = 1$ denotes the stoichiometric mixture, whereas $\phi = 0.5$ denotes the H_2/air mixture with twice the stoichiometric amount of air, and $\phi = 2$ is a mixture with half the stoichiometric amount of air necessary for complete combustion of the hydrogen content. The left-hand graph shows the ignition distance vs. temperature for all three mixtures at ambient pressure, whereas the right-hand graph shows exemplarily the ignition distance for the hydrogen-rich mixture ($\phi = 2$) at three different pressures of P = 1, 5, and 10 bar, respectively.

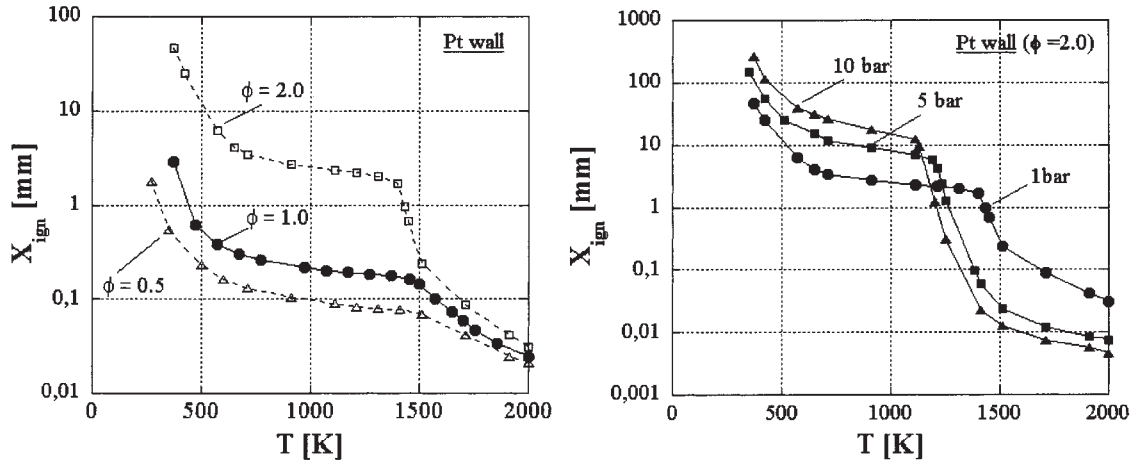

Figure 14. Left graph: Ignition distance vs. reaction temperature for a Pt-coated microchannel reactor (diameter: 300 μm) at 1 bar while varying the equivalence ratio ϕ from ϕ = 2.0 (open squares), ϕ = 1.0 (filled circles), to ϕ = 0.5 (open triangles). Right graph: ignition distance vs. temperature for fixed ϕ = 2.0, varying reactor pressure from 1 bar (circles), 5 bar (squares), to 10 bar (triangles).

All three ignition curves in the left graph show the same qualitative behavior, with the above-discussed transition from homogeneously dominated ignition at high temperatures to heterogeneously dominated ignition at lower temperatures. However, whereas the ignition distance at high temperatures is almost invariant against changes in equivalence ratio, the ignition distance for the low-temperature branch is strongly increased with increasing equivalence ratio.

This strong increase in ignition distance for the heterogeneous branch can be explained by the strongly increasing hydrogen partial pressure with increasing ϕ (P_{H_2} increases from 0.17 bar at $\phi = 0.5$ to 0.44 bar at $\phi = 2.0$). As mentioned earlier, Pt is essentially hydrogen poisoned before ignition of the reaction and the ignition process is thus dominated by the adsorption and desorption of hydrogen on the Pt surface.[37] Increasing hydrogen partial pressure shifts the adsorption/desorption equilibrium toward adsorption, exacerbating the blocking of the catalyst surface by H atoms, which thus results in an enhanced ignition delay.

Finally, to ascertain that the ignition behavior with regard to pressure changes as discussed above for stoichiometric mixtures is not affected in a qualitative way by changes in the fuel-to-air ratio, we conducted simulations of hydrogen oxidation in a Pt-coated 300-μm microchannel for several different pressures and equivalence ratios. Exemplary results for a hydrogen-rich mixture ($\phi = 2.0$) are shown in the right graph in Figure 14. One can see that the previously discussed results are not affected by changes in the fuel-to-air ratio: Similar to the behavior of a stoichiometric mixture (see Figure 7), the homogeneously dominated high-temperature ignition branch shifts toward shorter ignition distances with increasing pressure, whereas the heterogeneously dominated low-temperature ignition shifts toward longer ignition distances. This behavior was explained in detail above.

Overall, the behavior observed for a stoichiometric mixture of hydrogen and oxygen is thus not affected qualitatively by changes in the hydrogen-to-air ratio, and the main conclusions of this investigation therefore hold independent of the composition of a specific hydrogen/air mixture.

Summary and Conclusions

The ignition behavior of H_2 oxidation with air was studied in a microchannel reactor by numerical simulations with a 2D boundary-layer model coupled with detailed reaction kinetics both for catalytic surface reactions and for homogeneous gas-phase reactions. Platinum was selected as a well-studied, widely used oxidation catalyst, and results were compared with the purely homogeneous reaction behavior to identify the effect of the strongly enhanced homogeneous–heterogeneous interactions in the microscale dimensions of a micromachined reactor.

A strong influence of the catalytic wall on the ignition behavior of hydrogen–air mixtures was found. As expected, the catalytic wall leads to a strong acceleration of ignition for relatively low reaction temperatures ($T < 1000$ K) and extended the range of ignition toward much lower temperatures. At higher reaction temperatures ($T > 1000$ K), the ignition process becomes homogeneously dominated, although the catalytic wall leads to a significant additional ignition delay, that is, the catalyst acts as an ignition inhibitor as a result of strong radical scavenging. Because this radical quenching becomes increasingly dominant with decreasing microchannel diameter, sufficiently small microchannel diameters ultimately result in a complete quenching of homogeneous reactions, in good qualitative agreement with our previous experimental investigations.[19,21]

This quenching, however, is a strong function of reactor pressure. The parameter range in which an intrinsic (that is, temperature-independent) quenching exists for sufficiently small microchannel diameters can be calculated from a mathematical fitting procedure. For the present system we find this range to be bound to pressures $\lesssim 9.4$ bar, with a quenching diameter at ambient pressure of about 285 μm. Finally, the fuel-to-air ratio has no significant impact on the qualitative features, that is, on the nature of the interactions between heterogeneous and homogeneous reactions and the transition from a heterogeneously dominated to a homogeneously dominated ignition behavior.

The present study thus shed further light on one of the most interesting aspects of catalytic microreactors: because of the very large surface-to-volume ratio that can be realized in these systems, they can be manufactured to be *intrinsically* safe for highly explosive reactions. Many of the often-stated advantages of micromachined chemical reactors—such as the high heat and mass transfer rates and the intrinsic reactor safety arising from the small reactant volume present in the system at any moment—scale continuously with reactor size (or diameter). These characteristics thus do not necessarily require a true *micro*reaction system but can typically be attained in simple "minireactors," that is, compact, but conventional, reactor systems in which characteristic dimensions have simply been scaled down to sufficiently small dimensions, often in the centimeter to millimeter range. In contrast to that, the "intrinsic reactor safety" discussed in this contribution, that is, the temperature-independent quenching of homogeneous reactions, is an effect that requires characteristic dimensions below a critical diameter that is—for the present system—in the submillimeter range.

This effect has significant implications both for practical application and for scientific research. Safety issues associated with a potentially vastly expanded use of hydrogen in a future "hydrogen economy" are hotly debated these days, and the combustion of hydrogen is also pursued as a potential alternative to fuel cells for the use of hydrogen as a clean energy carrier. For both of these applications, the quenching of (uncontrolled) homogeneous reactions is crucial, and the presented results might yield a guideline for the design of containers and reactors with increased or even "intrinsic" safety.

On the scientific end, high-temperature catalysis is currently receiving much attention as a very efficient way to convert fossil and renewable hydrocarbon fuels. Here, a study of catalytic reaction mechanisms and kinetics without masking effects by homogeneous reactions is crucial and very difficult (if not impossible) to achieve in conventional "macroscopic" reactors. As demonstrated by the results of the present study, appropriately designed catalytic microreactors unambiguously allow us to discern catalytic from homogeneous reaction contributions, offering novel possibilities to achieve this goal.

Although the results of the presented simulation study obviously hold quantitatively only for the specific system (that is, hydrogen oxidation over platinum), it can be expected that

qualitatively similar quenching effects should be observable for many other wall materials as well as for wide range of chemically similar reaction systems, such as hydrocarbon oxidation reactions. We are currently extending our studies to investigate these aspects in detail.

Notation

c_{Pk} = specific heat at constant P of kth species, J kg^{-1} K^{-1}
P = pressure, N/m^2
r = radial (cross-stream) coordinate, m
s = sticking coefficient
T = temperature, K
u = axial velocity of fluid mixture (z direction), m/s
v = radial velocity of fluid mixture (r direction), m/s
$V_{k,r}$ = diffusion velocity of kth species in r direction, m/s
$\bar{W}$ = mean molecular weight of a mixture, kg/mol
W_k = molecular weight of the kth species, kg/mol
Y_k = mass fraction of the kth species
z = spatial coordinate along principal flow axis, m

Greek letters

λ = thermal conductivity of the gas mixture, J m^{-1} s^{-1} K^{-1}
μ = mixture viscosity, kg m[$^{\text{minus}1}$] s^{-1}
ρ = mass density of a gas mixture, kg/m^3
$\dot{\omega}_k$ = chemical production rate of kth species arising from gas-phase reactions, mol m^{-3} s^{-1}
ϕ = equivalence ratio
Θ_k = surface coverage of kth species

Literature Cited

1. Garibyan TA, Margolis LY. Heterogeneous–homogeneous mechanism of catalytic oxidation. *Catal Rev Sci Eng.* 1989;31:355-384.
2. Williams WR, Stenzel MT, Song X, Schmidt LD. Bifurcation behaviour in homogeneous–heterogeneous combustion. *Combust Flame.* 1991;84:277-291.
3. Ismagilov ZR, Pak SN, Yermolaev VK. Heterogeneous–homogeneous reactions involving free radicals in processes of total oxidation. *J Catal.* 1992;136:197-201.
4. Pfefferle LD. Heterogeneous/homogeneous reactions and transport coupling for catalytic combustion systems: A review of model alternatives. *Catal Today.* 1995;26:255-265.
5. Vislovskiy VP, Suleimanov TE, Sinev M, Tulenin YP, Margolis LY, Cortés Corberán V. On the role of heterogeneous and homogeneous processes in oxidative dehydrogenation of C3–C4 alkanes. *Catal Today.* 2000;61:287-293.
6. Zerkle DK, Allendorf MD, Wolf M, Deutschmann O. Understanding homogeneous and heterogeneous contributions to the platinum-catalyzed partial oxidation of ethane in a short-contact-time reactor. *J Catal.* 2000;196:18-39.
7. Veser G, Frauhammer J. Modelling steady state and ignition during catalytic methane oxidation in a monolith reactor. *Chem Eng Sci.* 2000;55:2271-2286.
8. Driscoll DJ, Campbell KD, Lunsford JH. Surface-generated gas-phase radicals: Formation, detection and role in catalysis. *Adv Catal.* 1987; 35:139-186.
9. Lunsford JH. The catalytic conversion of methane to higher hydrocarbons. *Catal Today.* 1990;6:235-259.
10. Lewis B, von Elbe G. *Combustion and Flames and Explosions of Gases*. New York, NY: Academic Press; 1987.
11. Williams FA. *Combustion Theory*. 2nd Edition. London, UK: Addison–Wesley; 1985.
12. Enomoto K, Kobayashi Y. Ignitability of hydrogen–air mixture by hot surface and hot gases. *Hydrogen Energy Prog.* 1981;2:1149-1163.
13. Griffin TA, Pfefferle LD. Gas phase and catalytic ignition of methane and ethane in air over platinum. *AIChE J.* 1990;36:861-870.
14. Vlachos DG. Homogeneous–heterogeneous oxidation reactions over platinum and inert surfaces. *Chem Eng Sci*. 1996;51:2429-2438.
15. Mueller MA, Yetter RA, Dryer FL. Flow reactor studies and kinetic modeling of H_2/O_2/NOx and $CO/H_2O/O_2$/NOx reactions. *Int J Chem Kinet*. 1999;31:705-724.
16. Ehrfeld W, Hessel V, Loewe H. *Microreactors: New Technology for Modern Chemistry*. Weinheim, Germany: Wiley-VCH; 2000.
17. Jensen KF. Microreaction engineering—Is small better? *Chem Eng Sci.* 2001;56:293-303.
18. Gavriilidis A, Angeli P, Cao E, Yeong KK, Wan YSS. Technology and applications of microengineered reactors. *Trans IChemE.* 2002;80A:3-30.
19. Veser G, Friedrich G, Freygang M, Zengerle R. Micro-Electro-Mechanical Systems (MEMS). *Proc ASME-DSC.* 1998;66:199-206.
20. Veser G, Friedrich G, Freygang M, Zengerle R. A simple and flexible microreactor for investigations of heterogeneous catalytic gas phase reactions. *Stud Surf Sci Catal.* 1999;122:237-246.
21. Veser G. Experimental and theoretical investigation of H_2 oxidation in a high-temperature catalytic microreactor. *Chem Eng Sci.* 2001;56: 1265-1273.
22. Aghalayam P, Bui PA, Vlachos DG. The role of radical wall quenching in flame stability and wall heat flux: Hydrogen–air mixtures. *Combust Theory Modell.* 1998;2:515-530.
23. Park YK, Aghalayam P, Vlachos DG. A generalized approach for predicting coverage-dependent reaction parameters of complex surface reactions: Application to H_2 oxidation over platinum. *J Phys Chem A.* 1999;103:8101-8107.
24. Aghalayam P, Park Y, Vlachos DG. Construction and optimization of complex surface reaction mechanisms. *AIChE J.* 2000;46:2017-2029.
25. Andrae JCG, Bjoernbom PH. Wall effects of laminar hydrogen flames over platinum and inert surfaces. *AIChE J.* 2000;46:1454-1460.
26. Kee RJ, Coltrin ME, Glarborg P. *Chemically Reacting Flow*. Hoboken, NJ: Wiley-Interscience; 2003.
27. Kee RJ, Rupley FM, Miller JA, Coltrin ME, Grcar JF, Meeks E, Moffat HK, Wang C, Adigun O, Houf WG, Chou CP, Miller SF. *CHEMKIN Collection*, Release 3.7. San Diego, CA: Reaction Design, Inc.; September 2002.
28. Smith GP, Golden DM, Frenklach M, Moriarty, NW, Eireneer, B, Goldenberg M, Bowman CT, Hanson RK, Song S, Gardiner, WC, Lissianski VV, Qin Z. GRI mechanism 3.0, http://www.me.berkeley.edu/gri_mech/
29. Janicke M, Holzwarth A, Fichtner M, Schubert K, Schüth F. A microstructured catalytic reactor/heat exchanger for the controlled catalytic reaction between H_2 and O_2. *Stud Surf Sci Catal.* 2000;130:437-444.
30. Cho P, Law CK. Catalytic ignition of fuel/oxygen/nitrogen mixtures over platinum. *Combust Flame.* 1986;66:159-170.
31. Giovangigli V, Smooke MD. Numerical modeling of tubular strained laminar premixed flames. *Combust Sci Technol.* 1987;53:23-29.
32. Warnatz J, Allendorf MD, Kee RJ, Coltrin ME. A model of elementary chemistry and fluid mechanics in the combustion of hydrogen on platinum surfaces. *Combust Flame.* 1994;96:393-406.
33. Friedle U, Veser G. Counter-current heat-exchange reactor for high temperature partial oxidation reactions. *Chem Eng Sci.* 1999;54:1325-1332.
34. Neumann D, Veser G. Catalytic partial oxidation of methane in a high-temperature reverse-flow reactor. *AIChE J.* 2005;51:210-223.
35. Veser G, Schmidt LD. Ignition and extinction in the catalytic oxidation of hydrocarbons over platinum. *AIChE J.* 1996;47:1077-1087.
36. Conaire MO, Curran HJ, Simmie JM, Pitz WJ, Westbrook CK. A comprehensive modeling study of hydrogen oxidation. *Int J Chem Kinet.* 2004;36:603-622.
37. Rinnemo M, Deutschmann O, Behrendt F, Kasemo B. Experimental and numerical investigation of the catalytic ignition of mixtures of hydrogen and oxygen on platinum. *Combust Flame.* 1997;111:312-326.
38. Ikeda H, Sato J, Williams FA. Surface kinetics for catalytic combustion of hydrogen–air mixtures on platinum at atmospheric pressure in stagnation flows. *Surf Sci.* 1995;326:11-26.

Manuscript received July 28, 2005, and revision received Feb. 7, 2006.